Simultaneous Single Site Color Photometry of LEO Satellites

James Frith, Brooke Gibson, Russell Knox, Kawailehua Kuluhiwa
Oceanit, Inc., Kihei, HI

ABSTRACT

Several Low Earth Orbit (LEO) satellites were observed simultaneously using three identically configured telescopes from the High-Accuracy Network Determination System (HANDS) at the Remote Maui Experiment (RME) observing site. Each telescope observed the satellites using a different Johnson filter (B, V, or R). In this way we acquired simultaneous color photometry of multiple LEO objects, and color indices were produced. We believe this approach will yield promising results in the field of non-resolved satellite characterization.

1. INTRODUCTION

Three identically integrated High-Accuracy Network Determination System (HANDS) telescopes [1], co-located at their temporary testing site at the Remote Maui Experiment (RME) in Kihei, Maui, were used for near simultaneous multi-filter observations on several Low Earth Orbit (LEO) objects. While there have been many multi-filter observations made of geosynchronous objects [2], color information about these continually changing and rapidly moving LEO objects can be difficult to capture using one system. In the time required to change from one filter to another, the satellite's phase angle and orientation have changed. Because HANDS is based on low cost, commercial off the shelf technology, having multiple co-located telescopes is feasible and part of the system's planned network architecture.

Our main goal is to produce light curves and temporal color indices. It has been shown that specular reflections take on the color of the source [3]. We will apply this combined with glint analysis to distinguish between specular and diffuse reflection by comparing the color of incident light source (the Sun) to the color of the reflected light. To this end, we observed three different types of LEO objects with cubical, spherical, and complex structures. The results we present in this paper are based on observations of LatinSat-A and Formosat 3D in the Johnson B, V, and R filters taken on December 19, 2007. An additional campaign was done on May 11, 2008, for which we present results on Lincoln Calibration Sphere 1 (LCS-1) in the B and V filters. Additional benefits of these observations include a test of the photometric capabilities of these standard, autonomous HANDS systems whose primary mission to provide metrics is currently evolving into autonomous LEO tracking and satellite photometry.

2. DATA COLLECTION

The HANDS systems used in the December observations comprised an RC Optical Systems Ritchey-Chrétien 16-inch telescope with a focal reducer, an Apogee Alta U47 1024x1024 back-illuminated charge-coupled device (CCD), an eight-position filter wheel with Johnson BVRI and Clear filters, and a German equatorial mount. The resulting field of view is 18 arcminutes wide. The telescopes were located in close proximity of one another, less than 100 feet apart, allowing for minimal variation in each system's perspective of the objects. In the May observations, only two telescopes were available. One had the same specifications previously described, and the other contained a Celestron Schmidt-Cassegrain 14-inch telescope with a focal reducer, providing a field of view of 20 arcminutes. The B and V filters were selected, based upon the preliminary results from December's observations which proved to be more revealing than the other color indices.

Software Bisque, CCDSoft Image and Camera Control Software, TheSky Astronomy Software, and Orchestrate were used for imaging and tracking during the data collection. Landolt calibration star fields [4], flat, dark, bias images, and LEO objects of interest were manually acquired in 3x3 binning mode in order to achieve more rapid frame rates. The effective superpixel size was 3.2 arecsec square. For dusk sky flats, the telescope was slewed to a specific altitude and azimuth defined as the declination equal to the site latitude and an hour angle of two hours east of the meridian which was found to have a minimal brightness gradient across the field. A series of fifty bias images and twenty 0.5 second dark images were obtained following flat images.

Two line element (TLE) sets for the LEO objects were acquired from the Space Track website [4] for tasking the observations. As a LEO object became visible, each of the observers began tracking it after it rose to 15 degrees above the horizon. The timing of the observations was coordinated with a predefined schedule in order to keep the observations as nearly simultaneous as possible.

Data on each LEO object were collected with exposure times of 0.5 seconds in order to collect sufficient light and avoid shutter effects. The time between subsequent frames is 2.35 seconds; this dictates the temporal resolution of the measurements. The length of a LEO's pass is dependent on its maximum elevation. In our case, we captured LEO passes ranging anywhere from two minutes to twenty minutes. In addition, we observed two passes of the same LEO object in one night such as LCS-1. The tables below summarize the LEO objects acquired and used in our analysis, as well as additional LEO objects we tracked.

Table 1: LEO objects obtained and used in our analysis

LEO Objects	Date	Filters
LatinSat-A	2007.12.19	B V R
Formosat 3D	2007.12.19	B V R
LCS-1	2008.05.11	B V

Table 2: Additional LEO objects that were tracked

Other LEO Objects Attempted	Date	Filters
CFESat Falconsat 3 Formosat 3B LatinSat-D	2007.12.12	B V R
LatinSat-A SaudiSat 1A	2007.12.18	B V
LCS-1 Picosat 9	2007.12.19	B V R VR
CFESat Falconsat 3 LatinSat C Unisat 3	2008.05.11	B V
CFEsat Cosmos 1249 Falconsat 3 LCS-1 LCS-4	2008.05.12	B V

Landolt star fields, for which the exoatmospheric magnitudes are precisely known, were acquired from 1 to 2.5 air masses in between or after LEO tracking.

3. ANALYSIS

Following the observations, all images were bias and dark corrected and flat-fielded. This was done in MatLab using conventional methods [6].

To find the exoatmospheric magnitude of the object of interest, the following basic equation is applied:

$$m_E = m_I - k_f X + C_f \tag{1}$$

where m_E is the exoatmospheric magnitude of the object, m_I is the instrumental magnitude, k_f is the extinction coefficient for filter *f*, *X* is the air mass, and C_f is the nightly offset for filter *f*. Since all of the constants and variables are filter-dependent except for *X*, the subscript *f* is used.

In order to find m_E, first C_f , k_f and *X* need to be determined. *X* is automatically calculated by Software Bisque and added to the image header, so it is a known quantity.

C_f and k_f are found using images of Landolt calibration stars with known magnitudes taken over a few air masses. The instrumental magnitude of the standard stars was measured using Source Extractor (SExtractor)[7]. The airmass was taken from the image header. C_f and k_f were then determined using a MatLab script which uses the least squares equation below:

$$k_f = \frac{n * \sum_{j=1}^{n} (m_L - m_I)_j * X_j - \sum_{j=1}^{n} (m_L - m_I)_j * \sum_{j=1}^{n} X_j}{(\sum_{j=1}^{n} X_j)^2 - n * \sum_{j=1}^{n} X_j^2}$$

$$C_f = \frac{\sum_{j=1}^{n} (m_L - m_I)_j * X_j * \sum_{j=1}^{n} X_j - \sum_{j=1}^{n} (m_L - m_I)_j * \sum_{j=1}^{n} X_j^2}{(\sum_{j=1}^{n} X_j)^2 - n * \sum_{j=1}^{n} X_j^2} \tag{2}$$

where *n* is the total number of images for the filter *f* and m_L is the Landolt magnitude.

Fig. 1 shows m_E - m_I vs. airmass and the least squares fit used to determine k_V and C_V for the observations in May of 2008.

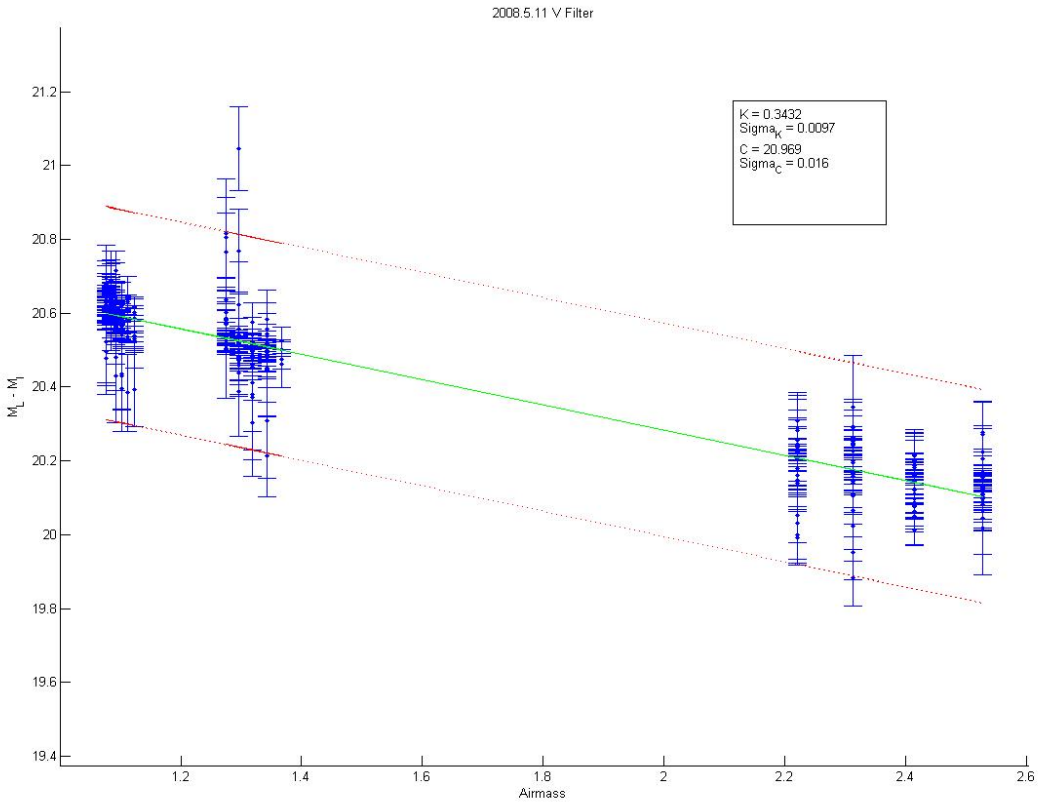

Fig. 1: Plot showing best fit line for determination of extinction coefficient and nightly offset. Error bars are 1 sigma.

With C_f and k_f, we find the instrumental magnitude, m_I, of the object and plug it back into equation (1). This gives us the exoatmospheric magnitude of the object, m_E. The objects of interest are detected within the data frames using SExtractor. Then an in-house sorting routine designed in MatLab parses the SExtractor output to obtain the instrumental magnitudes. Only objects at an airmass of 3 or lower were considered for this paper.

SatView, a program that takes TLEs as input to produce orbital information, was used to determine the object's range. When the range was determined and correlated with the time and exoatmospheric magnitude, the following equation was applied to normalize the object's range to 1000km:

$$M_f = M_E - 2.5 * \log_{10}\left(\frac{R_o^2}{R_n^2}\right) \tag{3}$$

where M_f is the final, range normalized, exoatmosphereic magnitude, R_o is the range output from SatView, and R_n, in this case, is 1000km.

The observations in each filter occurred at slightly different times. This is partly due to the limitations of the current tasking capabilities of our systems to task multiple systems with simultaneous observations. To compromise for this, linear interpolation was used to estimate values between the data points, which were also used to produce the B-V and V-R color indices. The resulting uncertainties in the filter specific magnitudes were +/- 0.10 and a color index uncertainty of +/-0.14.

4. RESULTS

Once range normalized and photometrically calibrated magnitudes have been obtained, the magnitudes can be graphed against many different variables. We plot magnitude and color indices against universal time (UT) below.

Lincoln Calibration Sphere 1 (LCS-1) is a polished aluminum sphere with a diameter of 1.13m. Past photometric observations have found it to be highly specular object [8]. Fig. 2 shows the expected result for a specular object in that its reflected light is very similar in color to the source of illumination (the Sun). During the time of observation, LCS-1 had a median B-V value of 0.64 where the Sun has a B-V value of 0.65. These are shown in the lower plot of Fig. 2.

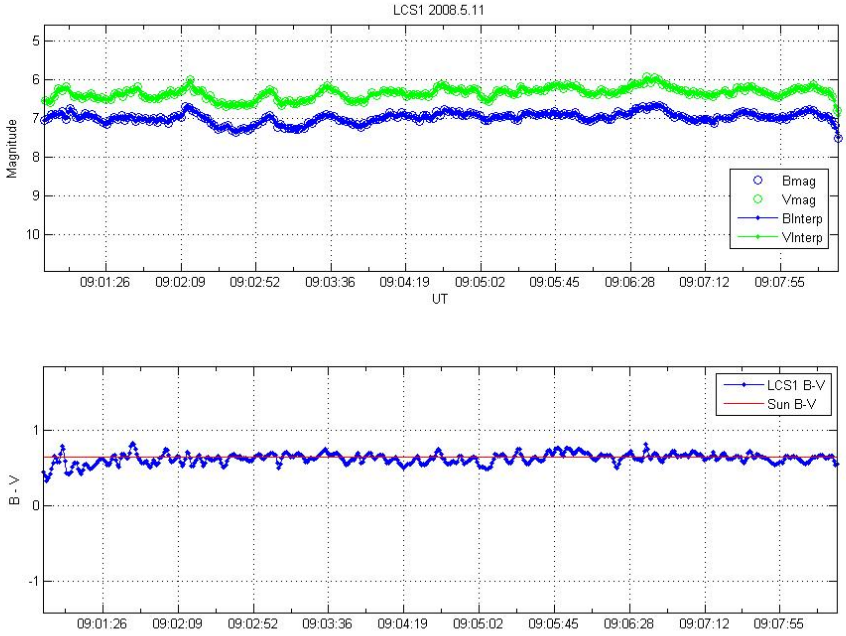

Fig. 2: Temporal plots of magnitude (top) and B-V color index (bottom) for the second pass of LCS-1 on 2008 May 11. Note the red line in the bottom graph showing the B-V value of the Sun. Uncertainties in measurements are +/- 0.10 magnitudes (top) and +/-0.14 (bottom).

LatinSat-A is a cube satellite with antennae and solar panels covering most of its surface. Fig. 3 shows R, B, and V light curves from December 2007. Three glints were observed in each of the three colors; the glints are separated by approximately 40 seconds.

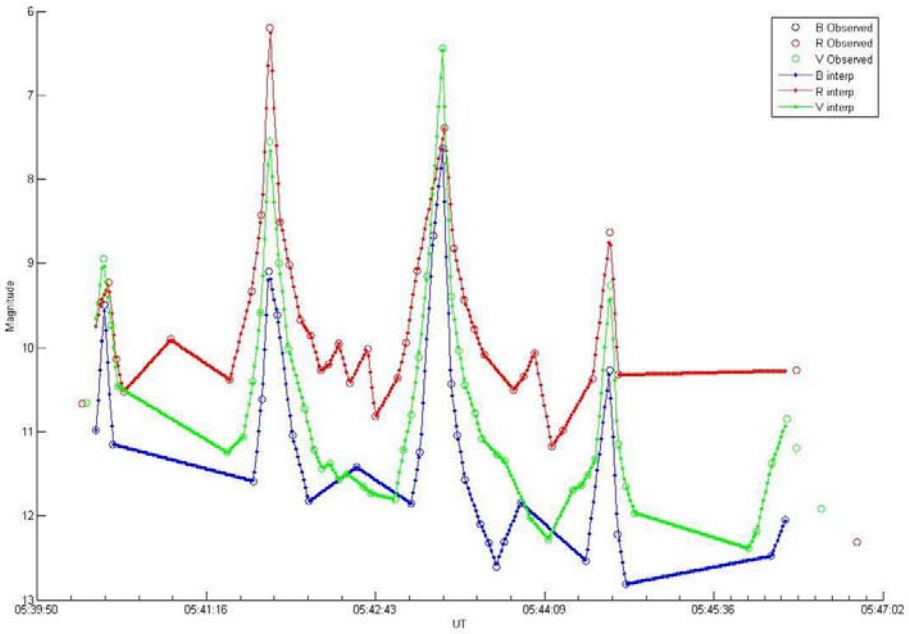

Fig. 3: Magnitude vs. time for LatinSat-A (cube) on 2007 December 19. The uncertainty in the measurements is +/- 0.10 magnitudes.

Fig. 4 shows that the B-V indices rapidly changed, appearing to redden during the glints. Effects in V-R space were not apparent. The fluctuations in the B-V values during the glints imply a difference in color between the specular and diffuse components of the object's reflected magnitude. Here, the B-V value during one glint changes from -0.1 to 1.2.

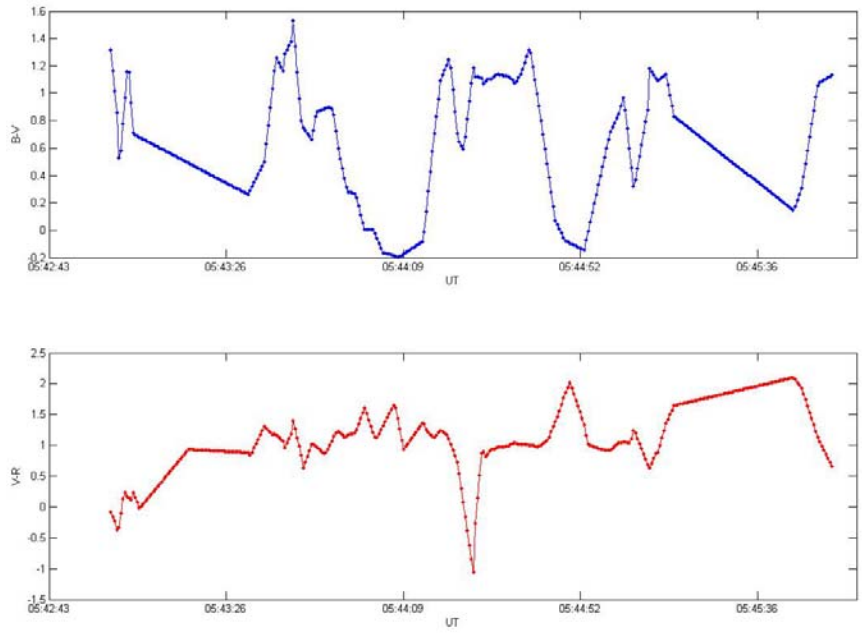

Fig. 4: Temporal plots of B-V and V-R color indices for LatinSat-A on 2007 December 19. Uncertainties are +/- 0.14.

Formosat 3D was also observed in December. Formosat 3D is an irregularly shaped object with many different materials and facets covering its surface. The light curves in Fig. 5 and corresponding color indices in Fig. 6 are irregular as expected.

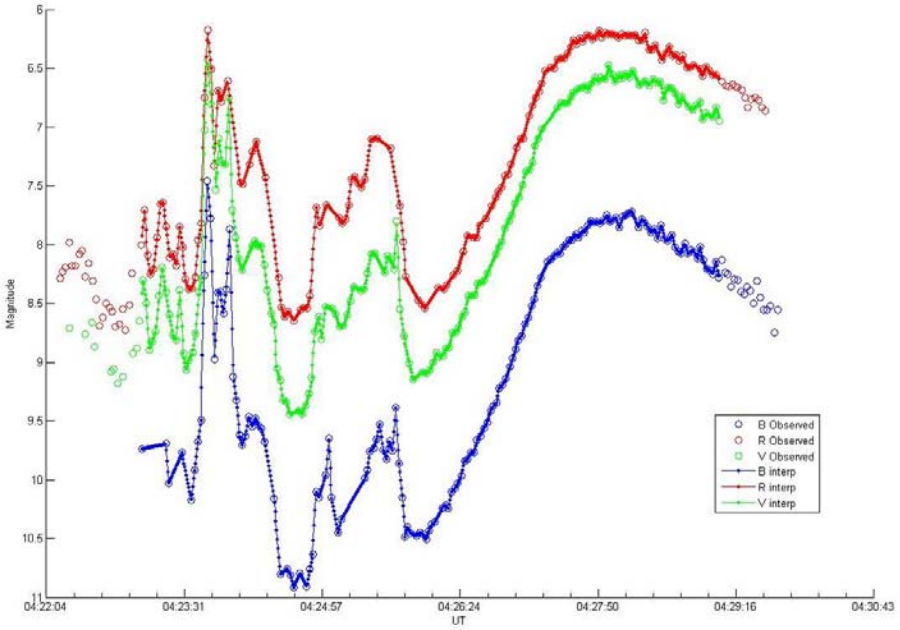

Fig. 5: Magnitude vs time for Formosat 3D on 2007 December 19 Uncertainties are +/-0.10 magnitudes.

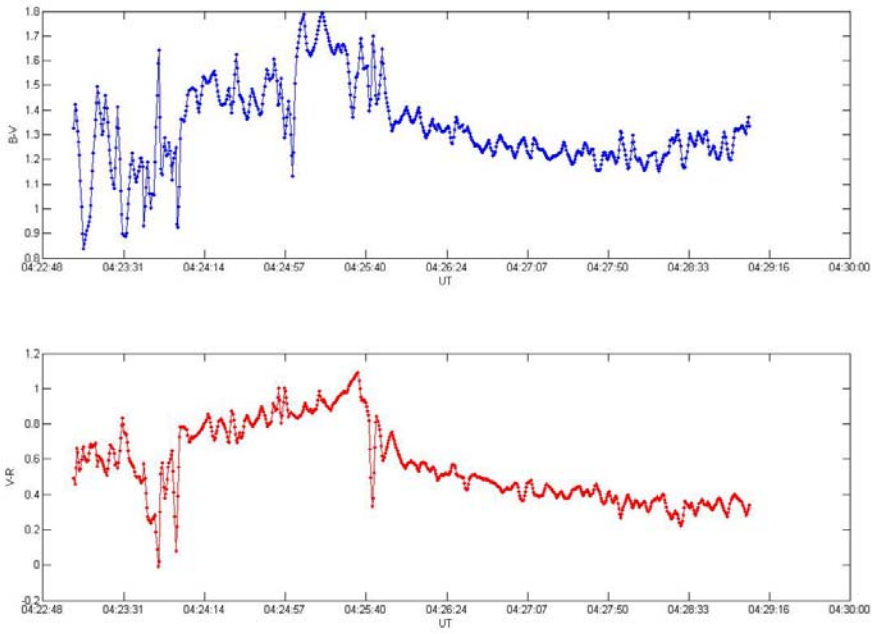

Fig. 6: Temporal plots of B-V and V-R color indices for Formosat 3D on 2007 December 19. Uncertainties are +/- 0.14.

5. CONCLUSIONS AND FUTURE WORK

The preliminary results indicate that color indices may enable the distinction between specular and diffuse reflections, at least for simple objects that are not self-shadowing. More observations, as well as more theoretical work, need to be done to better predict color index change as a function of an object's Bi-directional Reflectance Distribution Function (BRDF).

Our research also provides insight into the modifications required of a standard HGS to enable it to perform autonomous LEO tracking and to produce satellite photometry. Our recommendations include: a higher frame rate camera to improve time resolution and simultaneity in the observations, especially in the concurrency of glints in each filter; an alt-az mount to enable tracking of LEO objects through the meridian; a cloud sensor for autonomous photometry; a dome flat system; and modifications to system tasking to ensure simultaneous observations from multiple sites.

We also consider modeling objects of interest using Time-domain Analysis Simulation for Advanced Tracking (TASAT) [9] and the multi-site photometric modeling code developed by the Maui High Performance Computing Center Software Application Institute for Space Situational Awareness which we anticipate would assist us in the development of our algorithms.

6. ACKNOWLEDGEMENTS

We would like to express our gratitude to Doyle Hall (The Boeing Company), Paul Kervin (AFRL), Tamara Payne, and Steve A. Gregory (The Boeing Company) for their support. This research was performed under AFRL Contract Number FA9451-04-C-0381.

7. REFERENCES

1. Sabol C., Kelecy T., Murai M., "Geosynchronous Orbit Determination Using the High Accuracy Network Determination System (HANDS)," AAS/AIAA Spaceflight Mechanics Conference, Wailea, Maui, HI, Feb. 8-12, 2004, AAS 04-216.
2. Payne T.A. , Gregory S. A. , Color photometry of geosynchronous satellites using the SILC filters, Proc. SPIE 4490, 194 (2001), DOI:10.1117/12.455426
3. Cook, R., Torrance K., A Reflectance Model for Computer Graphics; ACM Transactions on Graphics, Vol.1 No.1, 7-24
4. Landolt, A. U., UBVRI photometric standard stars around the celestial equator Astronomical Journal, vol. 88, Mar. 1983, p. 439-460.
5. http://www.space-track.org
6. Howell, S.B., *Handbook of CCD Astronomy*, Cambridge University Press, 2000.
7. Bertin, E.; Arnouts, S, SExtractor: Software for source extraction, Astronomy and Astrophysics Supplement, v.117, p.393-404
8. Hall D., Africano J.L., Lambert, J.V., and Kervin, P.W., Time Resolved *I*-Band Photometry of Calibration Spheres and NaK Droplets, JOURNAL OF SPACECRAFT AND ROCKETS, Vol. 44, 910-919, 2007.
9. Riker, J.F, Butts, R. R., The time-domain analysis simulation for advanced tracking (TASAT) approaches to compensated imaging, Atmospheric propagation and remote sensing; Proceedings of the Meeting, Orlando, FL, Apr. 21-23, 1992 (A93-37102 14-74), p. 548-560.